

Terminal group modification of alkylthio substituted small molecule donor materials for organic solar cells

Yi Li^a, Yuancong Zhong^a, Shuguang Wen^{b,*}, Yong Zhang^{a,c,*}, Renqiang Yang^b

^a Institute of Optoelectronic Materials and Technology, South China Normal University, Guangzhou, 510631, PR China

^b CAS Key Laboratory of Bio-based Materials, Qingdao Institute of Bioenergy and Bioprocess Technology, Chinese Academy of Sciences, Qingdao, 266101, PR China

^c Guangdong Engineering Technology Research Center of Low Carbon and Advanced Energy Materials, Guangzhou, 510631, PR China



ARTICLE INFO

Keywords:

Small molecular donor
Alkylthio side chain
Planar backbone
Terminal groups
Organic solar cells

ABSTRACT

Side chains and terminal groups have an important effect on photovoltaic performance of organic solar cells (OSCs) based on oligothiophene donor materials. In order to study the effect of alkylthio substituent and different terminal groups on photovoltaic properties, a series of small molecules were designed and synthesized. Molecule LS0 was modified by alkyl as side chains and 2-ethylrhodanine as terminal groups while LS1a, LS1b, LS2, LS3 were substituted with alkylthio side chains and capped with different terminal groups of 2-ethylrhodanine, 2-hexylrhodanine, 2-ethylhexyl cyanoacetate, and 1,3-indanedione, respectively. Compared with LS0, alkylthio substituted LS1a exhibited higher HOMO and LUMO due to more planar backbone. Capped with different terminal groups, LS1a, LS1b, LS2, and LS3 showed the different optical and photovoltaic properties. Among these molecules, OSCs based on LS1b showed the highest power conversion efficiency (PCE) of 8.38% while others showed PCE of 7.87%, 6.52%, 6.52%, and 4.65% for LS0, LS1a, LS2, and LS3, respectively. The results demonstrated that rational selecting side chains and terminal groups could be a promising strategy to promote the performance of small molecule-based OSCs.

1. Introduction

Solution-processed bulk heterojunction (BHJ) organic solar cells (OSCs), due to their merits of light weight, easy fabrication and flexibility, have been paid great attention for application in renewable energy [1–9]. During the research, diverse designed and optimized strategies were adopted to promote the development of OSCs, such as structure innovation of active layer materials [10–13], blending films morphology control [14–17], interfacial modification [18–20], and device architecture design [21,22], giving rise to the high power conversion efficiencies (PCE) over 14% [23] for polymer donor based OSCs (P-OSCs) and 10% [24,25] for small molecule donor based OSCs (S-OSCs). Though the highest PCE of S-OSCs lagged behind P-OSCs, the increasing attention of S-OSCs showed its unique advantages in OSCs field. For instance, the molecular weight of polymer is a distribution of molecular weights, judged by number-average molecular weight (M_n) and polydispersity index (PDI), which leads to the existence of various molecular weights during batch-to-batch production. And it has been reported that polymer molecular weight could affect molecular ordering and blended surface morphology, thus influencing

repeatability of optimized P-OSCs performance [26,27]. In comparison to the polymeric donor materials, small molecule donor materials possess well-defined structure and molecular weight, no batch-to-batch variation, and higher levels of purity [28–30].

Currently, the high efficiency small molecule donor materials are mainly based on A-D-A structure, with benzo[1,2-b:4,5-b']dithiophene (BDT) as central unit, and terthiophene capped with electron-withdrawing terminal groups as two arms [31–35]. During the study of small molecule donor materials, side chains modification and terminal group innovation are two common strategies to optimize the optical and photovoltaic properties of the materials. For side chains modification, a lot of previous works have proved that introducing alkylthio substituent can lower the highest occupied molecular orbital (HOMO) of small molecule donor materials, thus increasing the open circuit voltage (V_{oc}) of OSCs devices [31,33,36]. Zou et al. introduced alkylthio side-chains in the molecular π -conjugated backbone and found that BDTT-S-TRS has a better planarity backbone (simulation dihedral torsion angles $\theta_1 = 0.59^\circ$, $\theta_2 = 8.03^\circ$, $\theta_3 = -13.78^\circ$) than BDTT-S-TR ($\theta_1 = 21.60^\circ$, $\theta_2 = 14.39^\circ$, $\theta_3 = 12.20^\circ$) through theoretical calculations. The optimized OSC device based on BDTT-S-TRS exhibited a PCE

* Corresponding author. Institute of Optoelectronic Materials and Technology, South China Normal University, Guangzhou, 510631, PR China.

** Corresponding author.

E-mail addresses: wensg@qibebt.ac.cn (S. Wen), zycq@scnu.edu.cn (Y. Zhang).

<https://doi.org/10.1016/j.dyepig.2019.107653>

Received 21 April 2019; Received in revised form 20 June 2019; Accepted 20 June 2019

Available online 26 June 2019

0143-7258/© 2019 Elsevier Ltd. All rights reserved.

of 8.07% with a notable FF of 0.705 [37]. However, the optical and photovoltaic properties (such as absorption coefficient and charge-carrier mobility) of alkyl substituted BDTT-S-TR weren't contrasted and analyzed systematically with BSTT-S-TRS. In our work, two molecules LS0 (substituted with alkyl side chains) and LS1a (substituted with alkylthio side chains) were designed and synthesized to study their differences on the optical and photovoltaic properties.

Beyond side chains modification, selecting an appropriate electron-withdrawing terminal group also is vital for small molecule design, which could directly determine whether it would act as a donor or a acceptor. It has been reported that the electron-withdrawing terminal groups have a great influence on the molecular absorption, solubility, energy levels, molecular packing, charge mobility and the final device performance of the corresponding solar cells [38–42]. The strength of acceptor would directly affect material's band gap and energy levels. The structure of end-capped groups could influence material's solubility and molecular packing. In Chen's work [43], they designed and synthesized molecules, DIN7T, DINCN7T and DDIN7T, with incorporating 1,3-indanedione and the derivative of 1,3-indanedione units as terminal groups, and demonstrated that the acceptor units had a great effect on molecular solubility and packing mode. Besides, Wei's group [41] reported four molecules, namely, BT-RCN, BT-BA, BT-RA and BT-ID, and found that with the increased planarity of end-capped acceptor, the π - π stacking distance also decreased. Thus, the modification of acceptor units would be an effective approach to adjust the photovoltaic performance of small molecule materials.

In order to further optimize the performance of S-OSCs and study the influence of end-capped groups on the optical and photovoltaic properties of small molecule materials, the end-capped groups with different electron withdrawing properties were adopted. These molecules, named as LS1a, LS1b, LS2, and LS3, were capped with 2-ethylrhodanine, 2-hexylrhodanine, 2-ethylhexyl cyanoacetate, and 1,3-indanedione, respectively. Among these alkylthio side chains substituted small molecules, LS1b showed lower HOMO and LUMO, which can be attributed to the different electron withdrawing properties of these terminal groups. Devices using these molecules as donor and PC₇₁BM as acceptor were fabricated and optimized via solvent vapor annealing (SVA). PCEs of 7.87%, 6.52%, 8.38%, 6.52%, and 4.65% were achieved for LS0, LS1a, LS1b, LS2, and LS3, respectively.

2. Experiment

2.1. Materials and synthesis

The chemical structure of LS0, LS1a, LS1b, LS2, and LS3 are shown in Fig. 1 and the detailed synthetic procedures are described in the Supporting Information. All reactions and manipulations were carried out under argon atmosphere. Unless otherwise specified, all materials were purchased from commercial suppliers and used directly without any purification.

2.2. Measurements and instruments

¹H NMR and ¹³C NMR spectra were performed in a Bruker AVANCE-III 600 MHz spectrometer using solutions in CDCl₃ and chemical shifts were recorded in ppm units with TMS as the internal standard. UV-vis spectra were recorded on a Lambda 25 spectrophotometer. The electrochemical measurements were carried out under nitrogen on a deoxygenated solution of tetra-*n*-butylammonium hexafluorophosphate (0.1 M) in acetonitrile with a computer-controlled CHI660C electrochemical workstation, a Pt working electrode, a platinum-wire auxiliary electrode, and a saturated calomel electrode (SCE) as the reference electrode. Potentials were referred to the ferrocenium/ferrocene (Fc/Fc⁺) couple by using ferrocene as a standard. The HOMO levels of small molecules were determined using the oxidation onset value.

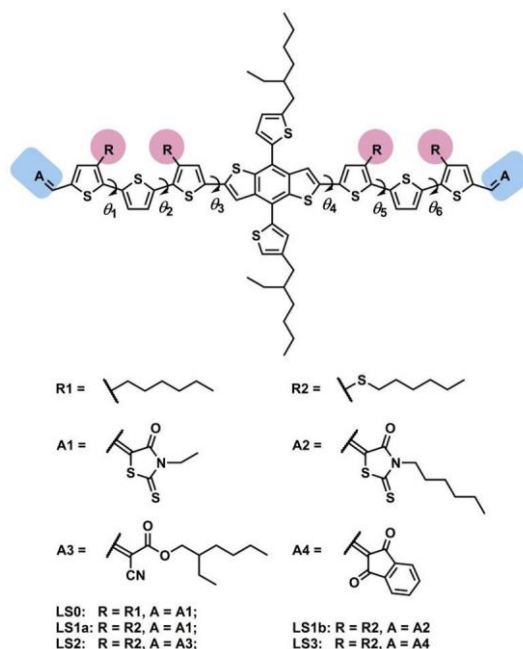


Fig. 1. Chemical structures of LS0, LS1a, LS1b, LS2, and LS3.

Topographic images of the active layers were obtained through atomic force microscopy (AFM) in tapping mode under ambient conditions using an Agilent 5400 instrument. Bright field transmission electron microscopy (TEM) images were acquired using a JEM-1400 PLUS electron microscope operating at an acceleration voltage of 120 kV. The space-charge-limited current (SCLC) mobility was measured using a configuration of ITO/PEDOT:PSS/donor:PC₇₁BM/MoO₃/Al for hole-only or ITO/ZnO/donor:PC₇₁BM/PFN/Al for electron-only devices by taking the dark current density in the range of 0–8 V.

2.3. Fabrication of devices

The S-OSCs devices were fabricated with a conventional architecture of ITO/PEDOT:PSS/small molecule:PC₇₁BM/PFN/Al. A solution of poly(3,4-ethylenedioxythiophene):poly(styrenesulfonate) (PEDOT:PSS) was spin-casted on pre-cleaned ITO coated glass at 4000 rpm and baked at 150 °C for 20 min in air to remove the residual solvent. Then the device was transferred into a nitrogen-filled glovebox. The small molecule and PC₇₁BM were dissolved in chloroform with a concentration of 6 mg/mL for small molecule. The optimum blend ratio of LS0:PC₇₁BM, LS1a:PC₇₁BM, LS1b:PC₇₁BM, LS2:PC₇₁BM, and LS3:PC₇₁BM is 1:0.8, 1:0.8, 1:1, 1:1.2, and 1:1.2, respectively. Then the blend chloroform solution was spin-coated on the top of PEDOT:PSS with a speed of 1500 rpm, 1000 rpm, 1500 rpm, 2000 rpm, and 2000 rpm for LS0:PC₇₁BM, LS1a:PC₇₁BM, LS1b:PC₇₁BM, LS2:PC₇₁BM, and LS3:PC₇₁BM, respectively. The thickness of small molecule and PC₇₁BM blend active layer was about 100 nm. The fresh molecule:PC₇₁BM blend films were put into the middle of a glass Petri dish containing 250 μ L chloroform for 30 s to undergo solvent vapor annealing (SVA). After SVA, the samples were taken out. PFN ethanol solution was subsequently spin-coated on the active layer. Finally, an Al metal top electrode (100 nm) was thermal evaporated under about 2×10^{-4} Pa. The active area of the device was 0.15 cm² defined by shadow mask. The current density-voltage (*J*-*V*) characteristics were measured with a Keithley 2400 source measurement unit under simulated 100 mW cm⁻² (AM 1.5 G) irradiation from a Newport solar simulator. Light intensity was calibrated with a standard silicon solar cell. The external quantum efficiencies (EQE) of solar cells were analyzed using a certified Newport incident photon conversion efficiency (IPCE) measurement system.

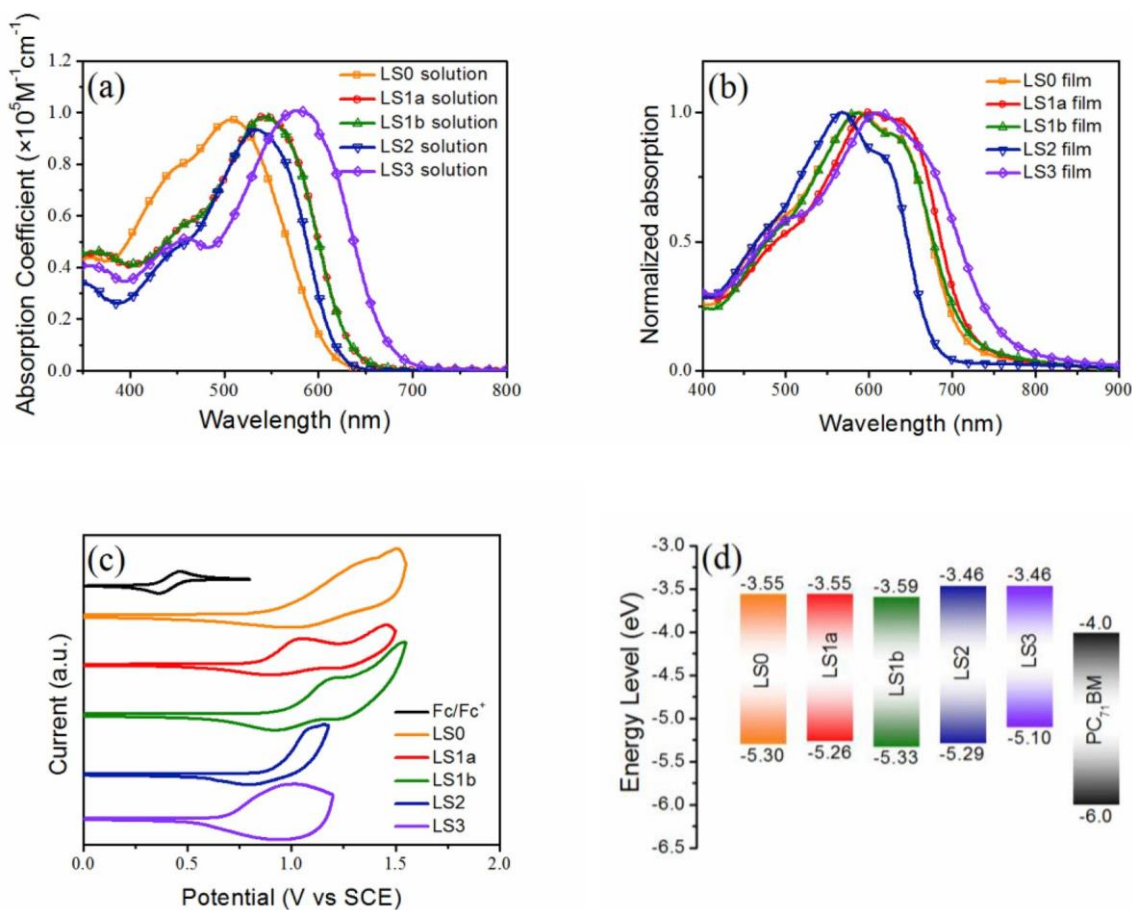


Fig. 2. Absorption spectra of small molecules in (a) chloroform solution and (b) films. (c) CV plots and (d) energy levels of the corresponding small molecules.

3. Results and discussion

3.1. Optical and electrochemical properties

Fig. 2(a) and (b) displayed the UV–vis absorption spectra of these five small molecules in dilute chloroform solution (10^{-5} M) and thin films. The detailed absorption properties, including absorption maxima, absorption onset and optical bandgap are summarized in Table 1. In dilute chloroform solution, these five molecules showed the absorption band ranging from 400 nm to 700 nm, and their absorption maxima peak were located at 511, 547, 547, 535, and 577 nm for LS0, LS1a, LS1b, LS2, and LS3, respectively. It could be observed that LS0 has more blue-shifted absorption and LS3 has more red-shifted absorption in dilute chloroform solution, compared to other molecules. The difference of absorption could be attributed to the different energy levels caused by molecular side chains and end-capped groups. The absorption coefficient also has been recorded in solution absorption. It can be seen that LS2 has lower absorption coefficient among these molecules, which could influence the short-circuit current (J_{SC}) of devices. In thin

films, these five molecules all have large red-shift in absorption spectrum due to the molecular aggregates. Calculated by the equation $E_g^{opt} = 1240/\lambda_{onset}$, the optical bandgap of LS0, LS1a, LS1b, LS2, LS3 were determined to be 1.75, 1.71, 1.74, 1.83, and 1.64 eV, respectively.

Cyclic voltammetry (CV) was employed to measure the HOMO and LUMO energy levels of these five molecules (Fig. 2(c)). The measurements were performed in an acetonitrile solution of 0.1 mol L^{-1} Bu_4NPF_6 by using ferrocene/ferrocenium (Fc/Fc^+) as the internal standard. And the formal potential of Fc/Fc^+ was measured as 0.41 V vs. SCE. The HOMO and LUMO levels of molecules were calculated from their onset oxidation potential (ϕ_{ox}) and the equation of $E_{LUMO} = E_{HOMO} + E_g^{opt}$ (eV) respectively. Thus, the HOMO and LUMO energy levels of these molecules were determined to be -5.30 and -3.55 eV for LS0, -5.26 and -3.55 eV for LS1a, -5.33 and -3.59 eV for LS1b, -5.29 and -3.46 eV for LS2, -5.10 and -3.46 eV for LS3, respectively. The HOMO offset and LUMO offset between small molecules and PC_{71}BM are over 0.3 eV, indicating enough driving force for exciton dissociation. In comparison with LS0, the HOMO and LUMO of molecule LS1a is slightly higher, which could be attributed to more

Table 1

Optical and electrochemical properties of small molecules.

Molecule	$\lambda_{sol-max}$ (nm)	$\lambda_{film-max}$ (nm)	$\epsilon_{sol-max}$ ($\text{M}^{-1}\text{cm}^{-1}$)	λ_{onset} (nm)	E_g^{opt} (eV)	HOMO ^a (eV)	LUMO ^b (eV)
LS0	511	588	9.71×10^4	709	1.75	-5.30	-3.55
LS1a	547	602	9.85×10^4	724	1.71	-5.26	-3.55
LS1b	547	583	9.82×10^4	714	1.74	-5.33	-3.59
LS2	535	568	9.31×10^4	677	1.83	-5.29	-3.46
LS3	577	609	1.01×10^5	758	1.64	-5.10	-3.46

^a Estimated from the onset of the oxidation potential.

^b Calculated by the equation $E_{LUMO} = E_{HOMO} + E_g^{opt}$ (eV).

Table 2
Simulated dihedral angles and energy levels of small molecules calculated by DFT/B3LYP/6-31G (d, p).

Molecule	θ_1	θ_2	θ_3	θ_4	θ_5	θ_6	HOMO (eV)	LUMO (eV)
LS0	-9.18	-17.09	9.55	-21.23	15.89	-7.31	-4.97	-2.85
LS1a	3.69	6.28	-7.14	21.20	-7.67	-4.08	-5.08	-2.96
LS1b	2.74	6.07	-9.50	20.07	-10.17	-6.39	-5.07	-2.94
LS2	3.66	5.88	-4.69	-20.39	1.08	-2.47	-5.16	-2.96
LS3	4.47	5.33	-5.88	21.25	-7.27	-3.36	-5.06	-2.92

planar backbone [44–47] of LS1a and electron-donating effect of alkylthio side chains. As shown in Fig. S1, the electronic distribution and geometrical configuration of LS0, LS1a, LS1b, LS2, and LS3 were calculated by density functional theory (DFT) at B3LYP/6-31G (d,p) level. The simulated dihedral angles of small molecules with optimized geometrical configuration were listed in Table 2. After insert sulfur atom into side chains, the values of θ_1 , θ_2 , θ_3 , θ_5 , and θ_6 in molecule LS1a were reduced significantly versus to LS0, indicating more planar backbone of LS1a. The energy levels of molecules were exhibited in Fig. 2(d). Influenced by different electron-withdrawing terminal groups, LS1a, LS1b, LS2, and LS3 showed differences in energy levels. In order to make clear the acceptor strength of these terminal groups, DFT also was carried out to calculate the dipole moment of acceptor units (as shown in Fig. S2.). In comparison with molecules LS1a, LS2, and LS3 (the dipole moments are 2.82 D, 2.02 D, and 1.46 D, respectively), LS1b showed relatively high dipole moment of 2.80 D, indicating the strong electron withdrawing ability of 2-hexylrhodanine, which was consistent with lower energy levels of LS1b.

3.2. Photovoltaic properties

To investigate the photovoltaic performance of the five small molecules, thin film BHJ solar cells were fabricated with a device structure of ITO/PEDOT:PSS/small molecule:PC₇₁BM/PFN/Al. Fig. 3 showed the current density–voltage (J–V) curves and the corresponding EQE spectra of the optimized devices under the illumination of AM 1.5 G at 100 mW cm⁻². The detailed photovoltaic performance parameters of the OPVs are listed in Table 3. Without any additional treatment, the PCE for LS0, LS1a, LS1b, LS2, and LS3, are 6.63%, 6.13%, 7.20%, 6.19%, and 4.14%, respectively. As displayed in Table 2, the main backbone substituted with alkylthio groups exhibited superior planarity than alkyl group. Therefore, the twist of molecular backbone of LS0 lead to a lower HOMO of LS0 than LS1a, inducing the higher V_{OC} of LS0 based devices. With the different electron withdrawing influence of terminal groups, molecule LS3 exhibited lowest V_{OC} among LS1a, LS1b, LS2, and LS3, consistent with its energy levels. As displayed in Table 3, after the treatment of chloroform solvent vapor annealing, the performances of these small molecules based devices have been significantly

improved. The performances of devices were increased from 6.63% to 7.87% for LS0, 6.13%–6.52% for LS1a, 7.20%–8.38% for LS1b, 6.19%–6.52% for LS2, and 4.14%–4.65% for LS3, respectively. The performance improvement could be mainly ascribed to the enhancement of J_{SC} and FF. Among these devices, the device based LS1b achieved the highest PCE of 8.38%, whereas devices based on LS2 or LS3 showed relatively lower J_{SC} . In Fig. S3, it could be observed that whether treated with SVA or not, devices based on LS2 or LS3 always exhibited relatively higher dark current density among these molecules, which could be accounted for the lower J_{SC} of LS2 and LS3. Fig. 3(b) displayed EQE spectra of the optimized devices based on these five molecules. The optimized devices exhibit a photon response from 300 nm to 700 nm, and the photocurrent generation of small molecule based devices is extended to higher wavelength in the order of LS2, LS0, LS1b, LS1a, and LS3, accordance with the absorption properties of these molecules. The J_{SC} -values calculated from the integration of the EQE data are consistent with the measured J_{SC} values, indicating the reliability of the photovoltaic results.

3.3. Mobility measurements

The charge-carrier mobility of active layer materials is important for S–OSCs. In order to further investigate the carrier extract and transport properties, SCLC measurements were performed to study the carrier mobility of the small molecule and fullerene blend films. The hole-only devices were fabricated as the structure of ITO/PEDOT:PSS/small molecule:PC₇₁BM/MoO₃/Al, while electron-only devices were fabricated with the structure of ITO/ZnO/small molecule:PC₇₁BM/PFN/Al. The J–V curves of hole-only devices and electron-only devices were shown in Fig. S4. The blend films based on the five small molecules and PC₇₁BM, without any additional treatment, exhibited the hole mobilities of 1.54×10^{-4} , 1.76×10^{-4} , 1.74×10^{-4} , 2.68×10^{-4} , and 3.01×10^{-4} cm²V⁻¹s⁻¹, and the electron mobilities of 1.06×10^{-4} , 8.93×10^{-5} , 1.19×10^{-4} , 2.18×10^{-4} , and 2.64×10^{-4} cm²V⁻¹s⁻¹ for LS0, LS1a, LS1b, LS2, and LS3, respectively. Influenced by side chains, LS1a with more planarity backbone showed higher hole mobility than LS0. After SVA treatment, the carrier-charge mobilities of the blend films showed a same rising trend. The hole and electron

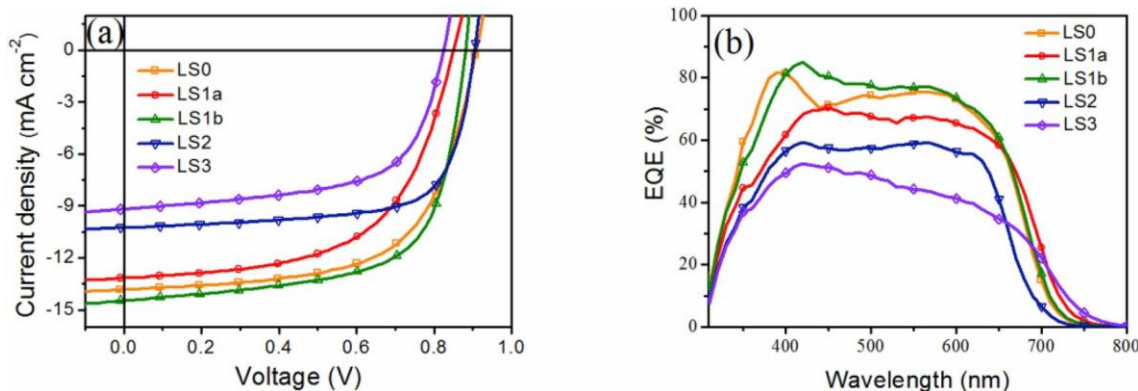
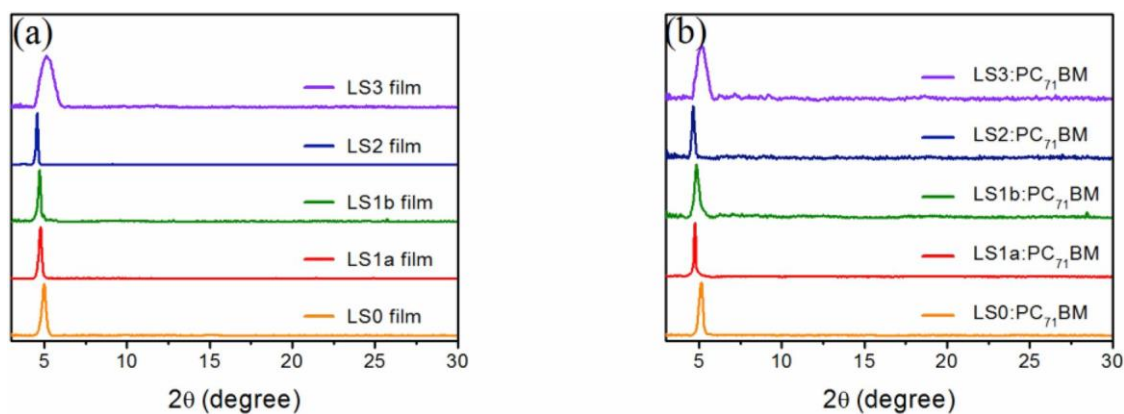
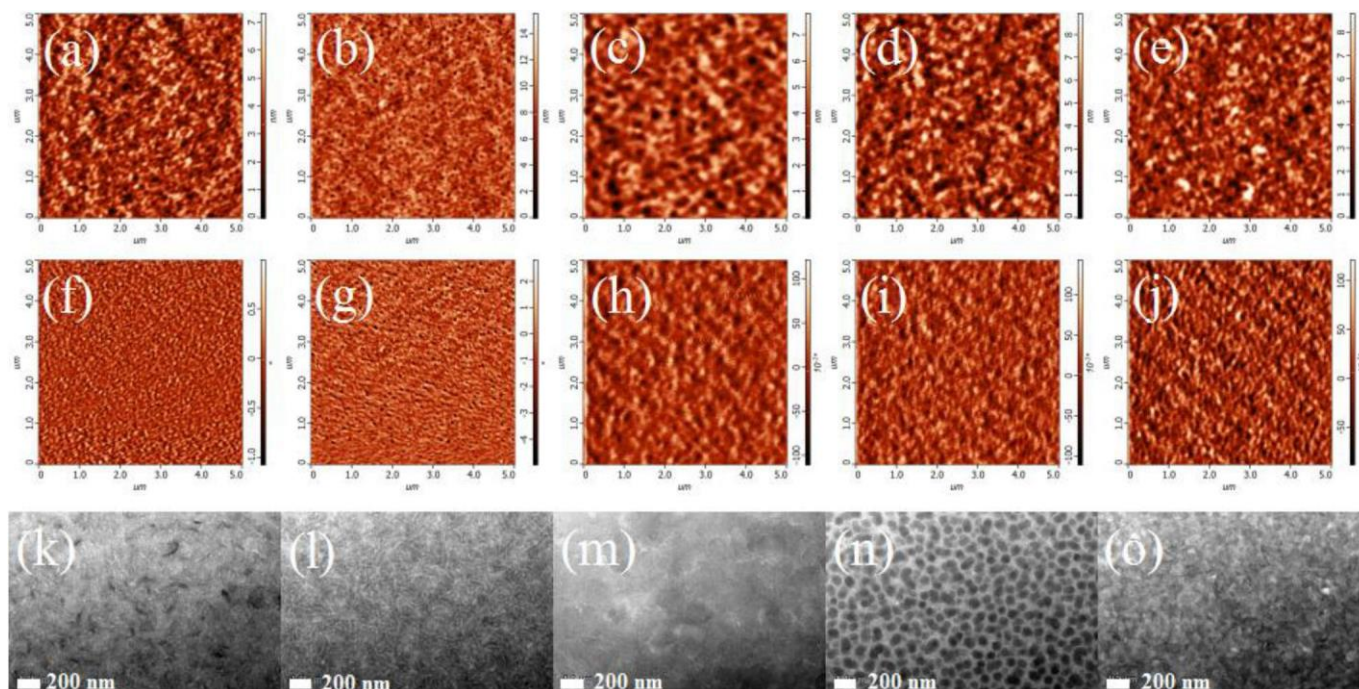


Fig. 3. Current density–voltage characteristics (a) and EQE spectra (b) of the optimized small molecule devices prepared based on the blend of small molecule and PC₇₁BM.

Table 3Photovoltaic parameters of the OPVs based on small molecule:PC₇₁BM under illumination of AM 1.5G, 100 mW cm⁻².

Active layer	D/A ratios	V _{oc} (V)	J _{sc} (mA cm ⁻²)	FF (%)	PCE _{max} (%)
LS0:PC ₇₁ BM ^a	1:0.8	0.935 (0.929 ± 0.007)	11.56 (11.43 ± 0.20)	61.35 (61.48 ± 0.36)	6.63 (6.47 ± 0.13) ^c
LS0:PC ₇₁ BM ^b	1:0.8	0.909 (0.912 ± 0.005)	13.83 (13.53 ± 0.18)	62.64 (62.70 ± 0.13)	7.87 (7.73 ± 0.09) ^c
LS1a:PC ₇₁ BM ^a	1:0.8	0.879 (0.880 ± 0.002)	11.61 (11.53 ± 0.07)	60.06 (60.20 ± 0.26)	6.13 (6.10 ± 0.03) ^c
LS1a:PC ₇₁ BM ^b	1:0.8	0.851 (0.852 ± 0.006)	13.15 (13.11 ± 0.10)	58.27 (57.97 ± 0.53)	6.52 (6.48 ± 0.05) ^c
LS1b:PC ₇₁ BM ^a	1:1	0.883 (0.885 ± 0.004)	12.56 (12.47 ± 0.08)	64.85 (64.57 ± 0.18)	7.20 (7.14 ± 0.04) ^c
LS1b:PC ₇₁ BM ^b	1:1	0.880 (0.884 ± 0.005)	14.46 (14.26 ± 0.12)	65.84 (65.67 ± 0.18)	8.38 (8.29 ± 0.07) ^c
LS2:PC ₇₁ BM ^a	1:1.2	0.906 (0.905 ± 0.002)	9.97 (9.93 ± 0.04)	68.44 (68.45 ± 0.14)	6.19 (6.15 ± 0.03) ^c
LS2:PC ₇₁ BM ^b	1:1.2	0.905 (0.910 ± 0.003)	10.26 (10.14 ± 0.07)	70.28 (69.83 ± 0.34)	6.52 (6.43 ± 0.06) ^c
LS3:PC ₇₁ BM ^a	1:1.2	0.822 (0.816 ± 0.004)	8.49 (8.42 ± 0.05)	59.39 (59.74 ± 0.28)	4.14 (4.10 ± 0.03) ^c
LS3:PC ₇₁ BM ^b	1:1.2	0.820 (0.820 ± 0.002)	9.18 (9.06 ± 0.16)	61.72 (61.52 ± 0.23)	4.65 (4.57 ± 0.07) ^c

^a Without any treatment.^b Treated with SVA.^c Average values with standard deviation were obtained from 10 devices.**Fig. 4.** XRD patterns of (a) the small molecule films and (b) small molecule:PC₇₁BM blend films.**Fig. 5.** AFM topography, phase morphology, and TEM images of blends films with SVA treatment: (a) (f) (k) LS0:PC₇₁BM, (b) (g) (l) LS1a:PC₇₁BM, (c) (h) (m) LS1b:PC₇₁BM, (d) (i) (n) LS2:PC₇₁BM, and (e) (j) (o) LS3:PC₇₁BM.

mobilities of the blend films are calculated to be 2.50×10^{-4} and $1.06 \times 10^{-4} \text{ cm}^2 \text{V}^{-1} \text{s}^{-1}$ for LS0, 1.99×10^{-4} and $9.46 \times 10^{-5} \text{ cm}^2 \text{V}^{-1} \text{s}^{-1}$ for LS1a, 3.15×10^{-4} and $2.37 \times 10^{-4} \text{ cm}^2 \text{V}^{-1} \text{s}^{-1}$ for

LS1b, 2.56×10^{-4} and $3.38 \times 10^{-4} \text{ cm}^2 \text{V}^{-1} \text{s}^{-1}$ for LS2, 3.12×10^{-4} and $2.40 \times 10^{-4} \text{ cm}^2 \text{V}^{-1} \text{s}^{-1}$ for LS3, respectively. After treated with SVA, most devices showed more balanced carrier transport, accounting

for the improvement of FF after SVA treatment. However, the device based on LS1a exhibited more unbalanced carrier transport and significantly low hole mobility, indicated that charges cannot be effectively extracted before recombination in the LS1a blend films, which might be one of the reason causing the low FF of LS1a based devices.

3.4. XRD and morphology analysis

The crystalline nature of the pristine small molecule films and small molecule:PC₇₁BM blend films was characterized by X-ray diffraction (XRD) analysis. As shown in Fig. 4, the small molecule films displayed high crystallinity with (100) diffraction peak at $2\theta = 4.99^\circ$, 4.77° , 4.71° , 4.56° , and 5.12° , and corresponding to a d_{100} -spacing of 17.71 Å, 18.50 Å, 18.73 Å, 19.39 Å and 17.23 Å for LS0, LS1a, LS1b, LS2, and LS3 respectively. Compared to LS0, alkylthio substituted LS1a exhibited slightly larger d_{100} -spacing, which could be ascribed to the insertion of S atom induced enlargement of side chains. For the films based on LS1a, LS1b, and LS2, with the alkyl chains length increasing on terminal groups, the d_{100} -spacing also gradually became larger. Owing to no sp³-hybridized atom on terminal groups in LS3, LS3 film showed minimized d_{100} -spacing among these films. After small molecules blended with PC₇₁BM, the blend films also exhibited obvious (100) diffraction peak with $2\theta = 5.14^\circ$, 4.75° , 4.85° , 4.64° , and 5.22° , corresponding to a d_{100} -spacing of 17.17 Å, 18.58 Å, 18.20 Å, 19.04 Å and 16.91 Å for LS0:PC₇₁BM, LS1a:PC₇₁BM, LS1b:PC₇₁BM, LS2:PC₇₁BM, and LS3:PC₇₁BM respectively.

Atom force microscope (AFM) and transmission electron microscope were conducted to further characterize the micromorphology of the active layer. The morphology images of the blend films with SVA treatment were displayed in Fig. 5. The root-mean-square (RMS) roughness values are 0.89, 1.25, 0.86, 1.05, and 1.07 nm for LS0:PC₇₁BM, LS1a:PC₇₁BM, LS1b:PC₇₁BM, LS2:PC₇₁BM, and LS3:PC₇₁BM blend films, respectively. Among these blend films, the film based on LS1a:PC₇₁BM showed substantial numbers of holes with slightly higher RMS in AFM images, indicating the inferior film-forming

ability. The worse film morphology of LS1a:PC₇₁BM blends could be a reasonable explanation for its lower electron mobility and FF. In the TEM images, these blend films exhibited different donor-acceptor

mixed morphology. For LS0:PC₇₁BM blends, there are large floc-like acceptor domains in the TEM images (Fig. 5(k)). For LS1a:PC₇₁BM and LS3:PC₇₁BM blends, the TEM images (Fig. 5(l) and (o)) showed crowded and large domains, caused by the inferior miscibility of donor and acceptor, which is unbeneficial for exciton separation and charge transfer. This lead to the low FF of LS1a:PC₇₁BM based devices and low J_{SC} of LS3:PC₇₁BM based devices. From Fig. 5(n), it can be observed definitely donor and acceptor interfaces in the image, similar with the figures reported in the literature [48]. For LS1b:PC₇₁BM blends, the film showed good donor-acceptor miscibility, which is beneficial for exciton separation and carrier transport.

4. Conclusion

In summary, five small molecule donor materials, named as LS0, LS1a, LS1b, LS2, and LS3, were designed and synthesized with different alkyl side chains and terminate groups. By replaced alkyl side chains with alkylthio side chains, LS1a showed higher energy levels and carrier mobility than LS0. Besides, through the simulated dihedral angles by DFT, it could be confirmed that inserting sulfur atom to side chains could increase molecular planarity. Influenced by different terminal groups, LS1b showed the lowest HOMO energy level among LS1a, LS1b, LS2, and LS3, indicating critical and effective energy levels modulation by rational end group selection. By altering side chains and end groups, these small molecules display a marked difference in aggregation behaviors, which can also be demonstrated by the film morphology when they are blending with PC₇₁BM. These differences synthetically con-

tribute to distinct photovoltaic performance with a maximum PCE of 8.38%, which provides directions on designing small molecules for OSCs.

Acknowledgements

This work was supported by the National Natural Science Foundation of China (No. 61574064), the Ministry of Science and Technology of China (2016YFE0115000), and the Science and Technology Planning Project of Guangdong Province (No. 2013CB040402009, 2015B010132009), the Science and Technology Project of Guangzhou City (No. 2014J4100056, 201607010250).

Appendix A. Supplementary data

Supplementary data to this article can be found online at <https://doi.org/10.1016/j.dyepig.2019.107653>.

References

- [1] Dai S, Zhan X. Nonfullerene acceptors for semitransparent organic solar cells. *Adv Energy Mater* 2018;8:1800002.
- [2] Kang Q, Ye L, Xu B, An C, Stuard SJ, Zhang S, et al. A printable organic cathode interlayer enables over 13% efficiency for 1-cm organic solar cells. *Joule* 2018;3:227–39.
- [3] Larrain FA, Fuentes-Hernandez C, Chou WF, Rodriguez-Toro VA, Huang TY, Toney MF, et al. Stable solvent for solution-based electrical doping of semiconducting polymer films and its application to organic solar cells. *Energy Environ Sci* 2018;11:2216–24.
- [4] Li D, Xiao Z, Wang S, Geng X, Yang S, Fang J, et al. A thieno[3,2-c]isoquinolin-5(4H)-one building block for efficient thick-film solar cells. *Adv Energy Mater* 2018;8:1800397.
- [5] Yang D, Sano T, Sasabe H, Yang L, Ohisa S, Chen Y, et al. Colorful squaraines dyes for efficient solution-processed all small-molecule semitransparent organic solar cells. *ACS Appl Mater Interfaces* 2018;10:26465–72.
- [6] Yang J, Lin Y, Zheng W, Liu A, Cai W, Yu X, et al. Roll-to-roll slot-die-printed polymer solar cells by self-assembly. *ACS Appl Mater Interfaces* 2018;10:22485–94.
- [7] A. Akkuratov, I. Martinov, I. Troshin. Impact of alkyl side chains on optoelectronic and photovoltaic properties of novel benzodithiophenedione-based (X-DADAD)_n conjugated polymers. *Phys Status Solidi RRL*. doi:10.1002/pssr.201900154.
- [8] Lu C, Chen H-C, Chuang W-T, Hsu Y-H, Chen W-C, Chou P-T. Interplay of molecular orientation, film formation, and optoelectronic properties on isoindigo- and thienoisoindigo-based copolymers for organic field effect transistor and organic photovoltaic applications. *Chem Mater* 2015;27:6837–47.
- [9] Chen W-C, et al. S,N-het-Chung C-L, Chen H-C, Yang Y-S, Tung W-Y, Chen J-W, eroacene-based copolymers for highly efficient organic field effect transistors and organic solar cells: critical impact of aromatic subunits in the ladder π -system. *ACS Appl Mater Interfaces* 2018;10:6471–83.
- [10] Gao W, Liu T, Ming R, Luo Z, Wu K, Zhang L, et al. Near-infrared small molecule acceptor enabled high-performance nonfullerene polymer solar cells with over 13% efficiency. *Adv Funct Mater* 2018;28:1803128.
- [11] Li X, Yao J, Angunawela I, Sun C, Xue L, Liebman-Pelaez A, et al. Improvement of photovoltaic performance of polymer solar cells by rational molecular optimization of organic molecule acceptors. *Adv Energy Mater* 2018;8:1800815.
- [12] Lee J, Ko SJ, Seifrid M, Lee H, Luginbuhl BR, Karki A, et al. Bandgap narrowing in non-fullerene acceptors: single atom substitution leads to high optoelectronic response beyond 1000 nm. *Adv Energy Mater* 2018;8:1801212.
- [13] Liao X, Yao Z, Gao K, Shi X, Zuo L, Zhu Z, et al. Mapping nonfullerene acceptors with a novel wide bandgap polymer for high performance polymer solar cells. *Adv Energy Mater* 2018;8:1801214.
- [14] McDowell C, Abdelsamie M, Toney MF, Bazan GC. Solvent additives: key morphology-directing agents for solution-processed organic solar cells. *Adv Mater* 2018;30:1707114.
- [15] Hu H, Li Y, Zhang J, Peng Z, Ma LK, Xin J, et al. Effect of ring-fusion on miscibility and domain purity: key factors determining the performance of PDI-based nonfullerene organic solar cells. *Adv Energy Mater* 2018;8:1800234.
- [16] Xie Y, Yang F, Li Y, Uddin MA, Bi P, Fan B, et al. Morphology control enables efficient ternary organic solar cells. *Adv Mater* 2018;30:1803045.
- [17] Jeon I, Delacou C, Okada H, Morse GE, Han TH, Sato Y, et al. Polymeric acid-doped

tribute to distinct photovoltaic performance with a maximum PCE of

- Y. Li, *et al.*, transparent carbon nanotube electrodes for organic solar cells with the longest doping durability. *J Mater Chem A* 2018;6:14553–9.
- [18] Zheng Z, Hu Q, Zhang S, Zhang D, Wang J, Xie S, et al. A highly efficient non- fullerene organic solar cell with a fill factor over 0.80 enabled by a fine-tuned hole- transporting layer. *Adv Mater* 2018;30:1801801.
- [19] Chou S-H, Chen H-C, Wang C-K, Chung C-L, Hung C-M, Hsu J-C, et al. Synthesis and characterization of new asymmetric thieno[3,4-*b*]pyrazinebased D- π -A-A type small molecular donors with near-infrared absorption and their photovoltaic applications. *Org Electron* 2019;68:159–67.
- [20] Dudem B, Jung JW, Yu JS. Improved light harvesting efficiency of semitransparent organic solar cells enabled by broadband/omnidirectional subwavelength antire- flective architectures. *J Mater Chem A* 2018;6:14769–79.

- [21] Kan B, Yi YQQ, Wan X, Feng H, Ke X, Wang Y, et al. Ternary organic solar cells with 12.8% efficiency using two nonfullerene acceptors with complementary absorptions. *Adv Energy Mater* 2018;8:1800424.
- [22] Cui Y, Zhang S, Liang N, Kong J, Yang C, Yao H, et al. Toward efficient polymer solar cells processed by a solution-processed layer-by-layer approach. *Adv Mater* 2018;30:1802499.
- [23] Zhang H, Yao H, Hou J, Zhu J, Zhang J, Li W, et al. Over 14% efficiency in organic solar cells enabled by chlorinated nonfullerene small-molecule acceptors. *Adv Mater* 2018;30:1800613.
- [24] Qiu B, Xue L, Yang Y, Bin H, Zhang Y, Zhang C, et al. All-small-molecule non-fullerene organic solar cells with high fill factor and high efficiency over 10%. *Chem Mater* 2017;29:7543–53.
- [25] Wan J, Xu X, Zhang G, Li Y, Feng K, Peng Q, et al. Highly efficient halogen-free solvent processed small-molecule organic solar cells enabled by material design and device engineering. *Energy Environ Sci* 2017;10:1739–45.
- [26] Katsouras A, Gasparini N, Koulgiannis C, Spanos M, Ameri T, Brabec CJ, et al. Systematic analysis of polymer molecular weight influence on the organic photovoltaic performance. *Macromol Rapid Commun* 2015;36:1778–97.
- [27] Mori H, Hara S, Nishinaga S, Nishihara Y. Solar cell performance of phenanthrothiophene–isoindigo copolymers depends on their thin-film structure and molecular weight. *Macromolecules* 2017;50:4639–48.
- [28] Collins SD, Ran NA, Heiber MC, Nguyen TQ. Small is powerful: recent progress in solution-processed small molecule solar cells. *Adv Energy Mater* 2017;7:1602242.
- [29] Roncali J, Leriche P, Blanchard P. Molecular materials for organic photovoltaics: small is beautiful. *Adv Mater* 2014;26:3821–38.
- [30] Sun Y, Welch GC, Leong WL, Takacs CJ, Bazan GC, Heeger AJ. Solution-processed small-molecule solar cells with 6.7% efficiency. *Nat Mater* 2011;11:44–8.
- [31] Cui C, Guo X, Min J, Guo B, Cheng X, Zhang M, et al. High-performance organic solar cells based on a small molecule with alkylthio-thienyl-conjugated side chains without extra treatments. *Adv Mater* 2015;27:7469–75.
- [32] Feng H, Li M, Ni W, Liu F, Wan X, Kan B, et al. Investigation of the effect of large aromatic fusion in the small molecule backbone on the solar cell device fill factor. *J Mater Chem A* 2015;3:16679–87.
- [33] Min J, Cui C, Heumueller T, Fladischer S, Cheng X, Spiecker E, et al. Side-chain engineering for enhancing the properties of small molecule solar cells: a trade-off beyond efficiency. *Adv Energy Mater* 2016;6:1600515.
- [34] Ji Z, Xu X, Zhang G, Li Y, Peng Q. Synergistic effect of halogenation on molecular energy level and photovoltaic performance modulations of highly efficient small molecular materials. *Nano Energy* 2017;40:214–23.
- [35] Yang Y, Wang K, Li G, Ran X, Song X, Gasparini N, et al. Fluorination triggered new small molecule donor materials for efficient as-cast organic solar cells. *Small* 2018;14:1801542.
- [36] Kan B, Zhang Q, Li M, Wan X, Ni W, Long G, et al. Solution-processed organic solar cells based on dialkylthiol-substituted benzodithiophene unit with efficiency near 10%. *J Am Chem Soc* 2014;136:15529–32.
- [37] Zou Y, Wu Y, Yang H, Dong Y, Cui C, Li Y. The effect of alkylthio side chains in oligothiophene-based donor materials for organic solar cells. *Mol Syst Des Eng* 2018;3:131–41.
- [38] Kose ME. Evaluation of acceptor strength in thiophene coupled donor-acceptor chromophores for optimal design of organic photovoltaic materials. *J Phys Chem A* 2012;116:12503–9.
- [39] He G, Li Z, Wan X, Zhou J, Long G, Zhang S, et al. Efficient small molecule bulk heterojunction solar cells with high fill factors via introduction of π -stacking moieties as end group. *J Mater Chem A* 2013;1:1801–9.
- [40] Li M, Ni W, Feng H, Wan X, Liu Y, Zuo Y, et al. A low bandgap carbazole based small molecule for organic solar cells. *Org Electron* 2015;24:89–95.
- [41] Deng D, Yang Y, Zou W, Zhang Y, Wang Z, Wang Z, et al. Aromatic end-capped acceptor effects on molecular stacking and the photovoltaic performance of solution-processable small molecules. *J Mater Chem A* 2018;6:22077–85.
- [42] Lee OP, Yiu AT, Beaujuge PM, Woo CH, Holcombe TW, Millstone JE, et al. Efficient small molecule bulk heterojunction solar cells with high fill factors via pyrene-directed molecular self-assembly. *Adv Mater* 2011;23:5359–63.
- [43] Zhang H, Yang X, Qiu N, Ni W, Zhang Q, Li M, et al. Oligothiophene based small molecules with a new end group for solution processed organic photovoltaics. *Org Electron* 2016;33:71–7.
- [44] Andersson MR, Thomas O, Mammo W, Svensson M, Theander M, Inganäs O. Substituted polythiophenes designed for optoelectronic devices and conductors. *J Mater Chem* 1999;9:1933–40.
- [45] Perez MD, Borek C, Forrest SR, Thompson ME. Molecular and morphological influences on the open circuit voltages of organic photovoltaic devices. *J Am Chem Soc* 2009;131:9281–6.
- [46] Andersson MR, Berggren M, Inganäs O, Gustafsson G, Gustafsson-Carlberg JC, Selse D, et al. Electroluminescence from substituted poly(thiophenes): from blue to near-infrared. *Macromolecules* 1995;28:7525–9.
- [47] Ko S, Hoke ET, Pandey L, Hong S, Mondal R, Risko C, et al. Controlled conjugated backbone twisting for an increased open-circuit voltage while having a high short-circuit current in poly(hexylthiophene) derivatives. *J Am Chem Soc* 2012;134:5222–32.
- [48] Deng D, Zhang Y, Zhu L, Zhang J, Lu K, Wei Z. Effects of end-capped acceptors subject to subtle structural changes on solution-processable small molecules for organic solar cells. *Phys Chem Chem Phys* 2015;17:8894–900.